CHEMISTRY OF MATERIALS
Cite This: Chem. Mater. 2018, 30, 1032−1044
Article
pubs.acs.org/cm

Synthesis of Supported Pd^0 Nanoparticles from a Single-Site Pd^{2+} Surface Complex by Alkene Reduction

Aidan R. Mouat,[†] Cassandra L. Whitford,[‡] Bor-Rong Chen,[§] Shengsi Liu,[†] Frédéric A. Perras,[∥] Marek Pruski,[∥] Michael J. Bedzyk,[§] Massimiliano Delferro,*[,†,#] Peter C. Stair,*[,†,⊥] and Tobin J. Marks*[,†,‡]

[†]Department of Chemistry, [‡]Department of Chemical & Biological Engineering, and [§]Department of Materials Science & Engineering, Northwestern University, Evanston, Illinois 60208, United States
[∥]U.S. DOE Ames Laboratory and Department of Chemistry, Iowa State University, Ames, Iowa 50011, United States
[⊥]Chemical Sciences & Engineering Division, Argonne National Laboratory, Lemont, Illinois 60439, United States

Supporting Information

ABSTRACT: A surface metal−organic complex, (-AlO_x)Pd(acac) (acac = acetylacetonate), is prepared by chemically grafting the precursor $Pd(acac)_2$ onto γ-Al_2O_3 in toluene at 25 °C. The resulting surface complex is characterized by inductively coupled plasma atomic emission spectroscopy (ICP-AES), X-ray photoelectron spectroscopy (XPS), X-ray absorption spectroscopy (XAS), and dynamic nuclear polarization surface-enhanced solid-state nuclear magnetic resonance spectroscopy (DNP SENS). This surface complex is a precursor in the direct synthesis of size-controlled Pd nanoparticles under mild reductive conditions and in the absence of additional stabilizers or pretreatments. Indeed, upon exposure to gaseous ethylene or liquid 1-octene at 25 °C, the Pd^{2+} species is reduced to form Pd^0 nanoparticles with a mean diameter of 4.3 ± 0.6 nm, as determined by scanning transmission electron microscopy (STEM). These nanoparticles are catalytically relevant using the aerobic 1-phenylethanol oxidation as a probe reaction, with rates comparable to a conventional Pd/Al_2O_3 catalyst but without an induction period. Diffuse reflectance infrared Fourier transform spectroscopy (DRIFTS) and temperature-programmed reaction mass spectrometry (TPR-MS) reveal that the surface complex reduction with ethylene coproduces H_2, acetylene, and 1,3-butadiene. This process reasonably proceeds via an olefin activation/coordination/insertion pathway, followed by β-hydride elimination to generate free Pd^0. The well-defined nature of the single-site supported Pd^{2+} precursor provides direct mechanistic insights into this unusual and likely general reductive process.

INTRODUCTION

Supported metal nanoparticles are an important class of heterogeneous catalysts[1,2] because they exhibit enhanced activity[3−5] and selectivity[6−8] compared to that of bulk metals. Nanoparticle size, particularly in the <6 nm regime,[9] markedly influences the catalytic properties of metal active sites as a consequence of both electronic and structural effects.[10,11] In such nanoparticles, undercoordinated edge and corner metal sites typically initiate catalytic transformations,[12] and metal−support interactions affect both the thermodynamic stability of nanoparticle size[13] and the strength of nanoparticle-adsorbate interactions.[14,15]

The influence of size, shape, and support interactions on nanoparticle reactivity[16] has prompted extensive investigation of methods to selectively prepare and stabilize nanoparticles in controlled size regimes of 1−15 nm.[17−20] In conventional syntheses of supported metal nanoparticles, a metal precursor is deposited on an appropriate support via an impregnation methodology and then reduced, typically at elevated temperature with H_2.[21] The reduction of dispersed metal species induces the formation of nanoparticles; however, these conditions must be carefully controlled since small nanoparticles are thermodynamically unstable and evolve toward the thermodynamic minimum of the bulk metal at elevated temperatures.[22−24] The tendency of nanoparticles to sinter therefore challenges the direct preparation of small, size-controlled nanoparticles on high-surface area supports.[25] Furthermore, while the stabilization of nanoparticle size and the suppression of sintering are active area research areas,[26,27] synthetic approaches are limited by a lack of understanding of the underlying sintering and agglomeration mechanisms.

An alternative approach to realizing nanoparticle catalysts is via the synthesis of colloidal nanoparticle suspensions, employing the reduction of a metal salt in the presence of an added coordinating capping agent or surfactant, to yield monodisperse particle size distributions.[28,29] Common capping agents include oleylamine,[30] oleic acid,[31] and functionalized polymers, such as polyvinylpyrrolidone (PVP).[31] Typical solution phase reducing agents include borane complexes,[32] hydrazine,[33] *n*-butyllithium,[34] or alcohols such as ethylene glycol.[35] Although these approaches are applicable to a variety of metal precursors and yield monodisperse nanoparticles, the

Received: November 22, 2017
Revised: January 2, 2018
Published: January 2, 2018

DOI: 10.1021/acs.chemmater.7b04909
Chem. Mater. 2018, 30, 1032−1044

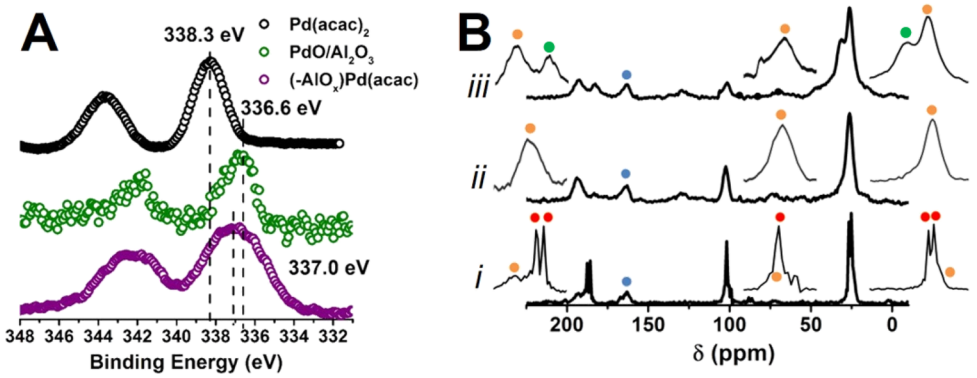

Figure 1. (A) Pd($3d_{5/2}$) XPS spectra of (-AlO_x)Pd(acac) (purple), PdO/Al_2O_3 (green), and Pd(acac)$_2$ (black). (B) DNP SENS $^1H-^{13}C$ CPMAS NMR of (i) (-AlO_x)Pd(acac), (ii) (-AlO_x)Pd(acac) after 96 h in 1-octene at 25 °C, and (iii) after 120 h in 1-octene at 25 °C. Red dots denote signals attributable to the (-AlO_x)Pd(acac) complex. Orange dots denote signals attributable to free acetylacetone on the alumina surface. Green dots represent an unidentified surface species, possibly surface acetate. Blue dots represent carbonate.

particles are only size-stable while they are surfactant-capped, limiting catalytic utility under typical reaction conditions.[25,36,37] While atomic layer deposition (ALD) using gaseous Pd(hfac)$_2$ (hfac = hexafluoroacetylacetonate) as a Pd precursor and formalin (37 wt % CH_2O/H_2O) as a reductant efficiently yields monodisperse 1−2 nm Pd nanoparticles at 200 °C,[38] this methodology effectively contaminates the surface of the nanoparticles with hfac and its fluorinated decomposition products,[39,40] which can compromise catalytic performance.

Additionally, a hybrid of the above two approaches has been explored in which surface grafting of well-defined organic or metal−organic fragments is used to control the structures and chemical properties of the resulting site-isolated species.[41−43] Based on previous work with single-site, oxide-supported early transition metal- and actinide-organic complexes,[44−47] we envisioned that supported late transition metal complexes might yield size-controlled metal nanoparticles under capping agent-free reductive conditions milder than conventional approaches.[48,49] Thus, methods for controlled grafting of vanadium and molybdenum acetylacetonates have been reported,[50] and the chemisorption of Pd(acac)$_2$ on γ-Al_2O_3 was investigated by van Veen[51] and De Jong[52] finding γ-Al_2O_3 surface chemistry similar to that reported from this laboratory.[53]

Here we report that contacting γ-Al_2O_3 with a toluene solution of Pd(acac)$_2$ at 25 °C yields the surface metal complex (-AlO_x)Pd(acac). This product is fully characterized by XPS, dynamic nuclear polarization (DNP) surface-enhanced solid-state NMR spectroscopy (SENS)[54−56] utilizing $^1H-^{13}C$ cross-polarization magic angle spinning (CPMAS), and by vibrational spectroscopy diffuse reflectance infrared Fourier transform spectroscopy (DRIFTS). In exploring conventional reductants, the reaction of (-AlO_x)Pd(acac) with H_2, hydrazine, borane complexes, and refluxing methanol in this lab yielded average Pd nanoparticle sizes greater than 9 nm. Formalin and sodium borohydride have also been employed as liquid-phase reductants for supported nanoparticle synthesis, but also result in larger metal particle sizes (6−10 nm).[57,58] In marked contrast, we report here that exposure of the (-AlO_x)Pd(acac) complex to either gaseous ethylene or liquid 1-octene, without adding capping or stabilizing agents at 25 °C, affords Pd^0 nanoparticles with a mean diameter of 4.3 ± 0.6 nm, as determined by bright field (BF-) and high angle annular dark field (HAADF-) STEM. Unlike conventional Pd/Al_2O_3 catalysts, the present nanoparticles are active for aerobic 1-phenylethanol oxidation without pretreament and exhibit no induction period.

These results demonstrate that surface metal−organic species and mild reductants can be used to prepare Pd nanoparticles of controlled size on high surface area supports without capping agents, surfactants, or ALD ligand fragments. Mechanistic evidence for this unusual reductive chemistry benefits from the well-defined, single-site nature of the supported Pd^{2+} precursor. Such mechanistic detail should provide greater insight into selective catalyst synthetic strategies, and addresses challenges in unravelling heterogeneous catalyst structure−function relationships.

RESULTS

Synthesis and Characterization of (-AlO_x)Pd(acac). The support material is a phase-pure, high-surface area γ-Al_2O_3.[53] The alumina was stirred under an inert atmosphere, in an anhydrous toluene solution of stoichiometrically excess Pd(acac)$_2$ overnight at 25 °C, yielding a beige, air-stable material having 0.20 wt % Pd, as determined by ICP-AES (see the Supporting Information for details), with the empirical formula (-AlO_x)Pd(acac). The low Pd loading achieved under these conditions suggests that there is significant reaction selectivity at 25 °C between Pd(acac)$_2$ and specific surface sites on the γ-Al_2O_3.[51]

As shown in Figure 1A (see also Figure S1 and Table S1), XPS confirms that the Pd center remains in the +2 oxidation state after grafting. The binding energy of the Pd($3d_{5/2}$) peak in Pd(acac)$_2$ is 338.3 eV in the local spectrometer, consistent with literature reports of similar compounds (e.g., Pd(acetate)$_2$).[59] A PdO/Al_2O_3 reference material was prepared by calcining (-AlO_x)Pd(acac) at 550 °C for 18 h under flowing O_2. After calcination, DNP-enhanced $^1H-^{13}C$ CPMAS spectra, which, for brevity, will be referred to as ^{13}C DNP SENS, indicate a complete decomposition of the initial surface complex (SI, Figure S2). The binding energy of the Pd($3d_{5/2}$) XPS peak for PdO/Al_2O_3 is centered at 336.6 eV, consistent with previous reports for PdO,[60] while the binding energy of the Pd($3d_{5/2}$) XPS peak for (-AlO_x)Pd(acac) is centered at 337.0 eV. These Pd($3d_{5/2}$) values are consistent with data for other Pd^{2+} complexes,[61] but correspond to neither the parent Pd(acac)$_2$ complex (338.3 eV) nor PdO/Al_2O_3 (336.6 eV) (Figure 1A) . The binding energy for Pd^0 is expected at 335.0 eV (vide infra).

DOI: 10.1021/acs.chemmater.7b04909
Chem. Mater. 2018, 30, 1032−1044

The presence of the surface (-AlO$_x$)Pd(acac) complex was confirmed via ^{13}C DNP SENS measurements (Figure 1B-*i*), performed using natural ^{13}C abundance. Sharp resonances corresponding to the methyl (−**C**H$_3$), methylene (−**C**H$_2$−), and carbonyl (−**C**=O) carbon species of the acac ligand are clearly visible. The resonances for the methyl and carbonyl carbons are doubled in a 1:1 ratio at δ = 27 and 25 ppm and 188 and 186 ppm, respectively, whereas the methylene carbon resonance is a singlet at δ = 102 ppm. In addition to the sharp, distinct peaks observed for the anchored surface complex, broad ^{13}C resonances at δ = 193, 101, and 24 ppm, characteristic of free acetylacetone,[62] are observed, confirming protonolysis of the (acac) ligand during the chemisorption of Pd(acac)$_2$ on γ-Al$_2$O$_3$. Adsorption of acetylacetone on γ-Al$_2$O$_3$ is further confirmed in DRIFTS experiments (vide infra) and is consistent with literature reports.[51] Other broad ^{13}C resonances appear at δ = 30, 163, and 183 ppm that cannot be attributed to acetylacetone, toluene, acetone, or the hexanes used in the synthesis. These signals are reasonably attributable to surface acetate and carbonate species, in agreement with TPD-MS results (vide infra), which show the liberation of acetone from the surface. Acetate and carbonate are assumed to arise from an interaction between a free or decomposed acac ligand and surface Lewis acid or hydroxyl groups.[63] As can be seen in Figures 1B-ii and -iii, signals from free acetylacetone become more apparent following the reduction of (-AlO$_x$)Pd(acac) (vide infra).[64]

Reduction of (-AlO$_x$)Pd(acac). The γ-Al$_2$O$_3$-supported surface Pd complex can be reduced with an alkene in either the gas or liquid phase at 25 °C. Three different reductive methods yield similar results: (a) suspending the (-AlO$_x$)Pd(acac) in 1-octene at 25 °C; (b) suspending the (-AlO$_x$)Pd(acac) in a hydrocarbon solvent (pentanes or toluene) and stirring under an ethylene atmosphere at 25 °C; or (c) exposing solid (-AlO$_x$)Pd(acac) to gaseous ethylene at temperatures from 25−50 °C. In this study, 1-octene is used as a liquid-phase reagent to monitor the reduction of the surface complex as a function of time, and ethylene is used as a vapor-phase reagent in spectroscopic and TPR experiments.

The reduction of (-AlO$_x$)Pd(acac) by 1-octene at 25 °C was monitored by XPS, XANES, and EXAFS. The XPS results for reaction durations of 6−120 h are depicted in Figure 2. The Pd(3d$_{5/2}$) peak for (-AlO$_x$)Pd(acac) is centered at 337.0 eV. A second feature at 335.0 eV increases in intensity during the reaction of (-AlO$_x$)Pd(acac) with 1-octene. This ionization

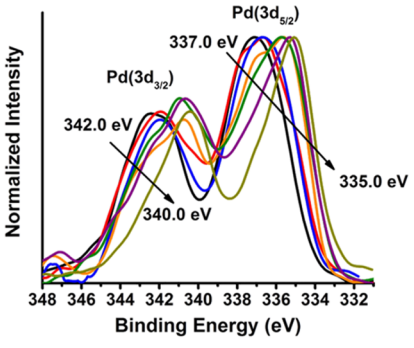

Figure 2. Pd(3d) XPS spectra of the parent (-AlO$_x$)Pd(acac) surface complex (black), and samples reduced with 1-octene at 25 °C for 6 (red), 24 (blue), 48 (orange), 72 (green), 96 (purple), and 120 h (yellow).

clearly indicates the formation of a new Pd species with a binding energy consistent with previous reports for Pd^0 species,[65] and correlates with both the appearance of Pd nanoparticles (by BF- and HAADF-STEM, vide infra) and the disappearance of (-AlO$_x$)Pd(acac), confirmed by ^{13}C DNP SENS (Figure 1B). The molar fractions of Pd^{2+} and Pd^0 were estimated by deconvoluting the two peaks in the XPS spectrum (Figure S1 and Table S1).

The presence of Pd^0 is further confirmed by Pd K-edge XANES (Figure 3A), which reveals that approximately 60% of the total palladium supported on the Al$_2$O$_3$ surface exists as Pd^0 after 120 h of reaction with 1-octene at 25 °C. EXAFS data and fits for (-AlO$_x$)Pd(acac) samples reduced for 0, 48, and 120 h in 1-octene at 25 °C are shown in Figure 3B. The EXAFS data are fit to the first coordination shell of fcc metallic Pd−Pd and Pd−O scattering paths.[66]

These results indicate that (-AlO$_x$)Pd(acac) has an average Pd−O coordination number (CN) ∼4, consistent with the proposed surface geometry (Chart 1; see more below) in which the Pd is directly bonded to three oxygen atoms and datively bonded to a vicinal hydroxyl group. These EXAFS data are in agreement with the results obtained from DNP SENS (vide supra, see Figure 1B). As the sample is reduced, the Pd−Pd coordination number increases, approaching 6 in the sample reduced for 120 h (Figures S12 and S13, Table S4).

The mechanism of (-AlO$_x$)Pd(acac) reduction was also investigated by DRIFTS under an ethylene atmosphere, as well as by TPR-MS analysis of the (-AlO$_x$)Pd(acac) + ethylene reaction products. Additionally, the presence of Pd nanoparticles is confirmed by BF-STEM imaging after the (-AlO$_x$)Pd(acac) + ethylene reaction at 50 °C (Figure S9). The absorbance-mode DRIFTS spectrum of (-AlO$_x$)Pd(acac) after reaction with ethylene at 50 °C is shown in Figure 4, backgrounded with a spectrum of (-AlO$_x$)Pd(acac) at 50 °C before exposure to ethylene. The broad negative feature at 3641 cm^{-1} indicates the consumption of water −OH groups during the reaction, presumably from H-bonding interactions with free acetylacetone ligand (vide infra). In the lower frequency region of the spectrum, sharp negative features appear at 1674, 1579, 1559, 1518, 1382, and 1275 cm^{-1}, while a single, broad positive feature appears at 1620 cm^{-1}. The negative features are assigned to the disappearance of the coordinated (acac) ligand from the surface complex,[51,67] while the feature at 1620 cm^{-1} is assigned to the carbonyl stretch of free acetylacetone.[51,68] The DRIFTS data therefore confirm that the (acac) ligand is detached during the (-AlO$_x$)Pd(acac) reduction and generates surface-bound acetylacetone as a product. These results strongly corroborate those obtained by DNP SENS (Figure 1B).

The organic products of the (-AlO$_x$)Pd(acac) + ethylene reduction reaction were also analyzed via TPR-MS (Figure 5). Acetylene, H$_2$, and 1,3-butadiene are the only products detectable in the reaction effluent. These products are consistent with coordination/insertion of the Pd center into the C−H bond of ethylene. The dimerization of ethylene is expected to yield 1.0 equiv. of 1,3-butadiene and 1.0 equiv of H$_2$, whereas β-hydride elimination and subsequent reductive elimination directly from a Pd-alkenyl complex is expected to yield 1.0 equiv of acetylene and a Pd^0 species.[69,70] By calibrating the integrated area (see the Supporting Information) of each gas-phase product using internal MS response factors, it can be seen that the molar ratio of 1,3-butadiene to H$_2$ is ∼1, whereas the ratio of acetylene to H$_2$ is ≫1, which supports the

DOI: 10.1021/acs.chemmater.7b04909
Chem. Mater. 2018, 30, 1032−1044

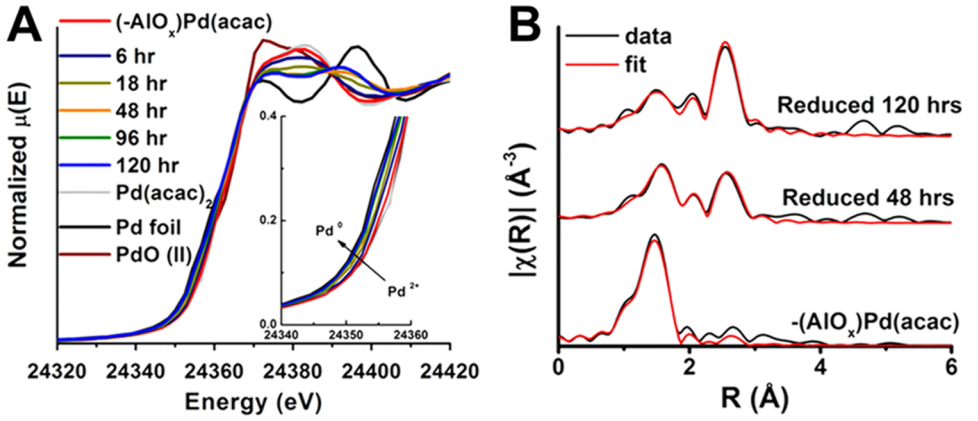

Figure 3. (A) XANES Pd K-edge spectra at various reduction times in 1-octene at 25 °C. Increasing Pd^0 character is noted in the inset figure. (B) EXAFS data and fits for parent (-AlO_x)Pd(acac) and samples reduced for 48 and 120 h in 1-octene at 25 °C.

Chart 1. Proposed Structure of the (-AlO_x)Pd(acac) Surface Complex, With the Pd Center Datively Interacting with a Surface Aluminol; The Observed acac Ligand Asymmetry Is Explained by the H-Bonding

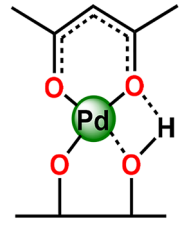

(-AlO_x)Pd(acac)

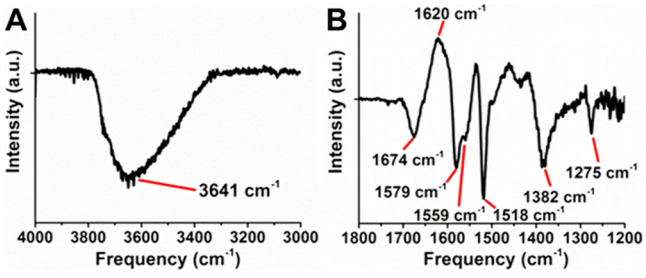

Figure 4. (**A**) Hydroxyl region (4000−3000 cm^{-1}) of the DRIFTS spectrum of (-AlO_x)Pd(acac) after reaction with ethylene at 50 °C. (**B**) Carbonyl region (1800−1200 cm^{-1}) of the DRIFTS spectrum of (-AlO_x)Pd(acac) after reaction with ethylene at 50 °C.

suggested reduction pathway (vide infra). No acetone is observed during the reaction, arguing that the decomposition of the acac ligand does not play a significant role in the reduction process. Interestingly, the production of acetylene, H_2, and butadiene ceases after ∼1 h, indicating that only (-AlO_x)Pd(acac) is capable of activating ethylene and effecting the reduction process. After the reaction, temperature-programmed desorption-mass spectrometry (TPD-MS) of the sample detects acetone (m/z = 58) above 200 °C, but no other surface-bound products, again in good agreement with DNP SENS (Figure 1B) as well as DRIFTS results (Figure 4).

Formation of Pd^0 Nanoparticles. The reduction of (-AlO_x)Pd(acac) in the presence of alkenes, and the conversion of Pd^{2+} to Pd^0, yields Pd nanoparticles, observable by BF- and HAADF-STEM. Figure 6A, B show the alumina surface and (-AlO_x)Pd(acac) without nanoparticles as observed by BF- and

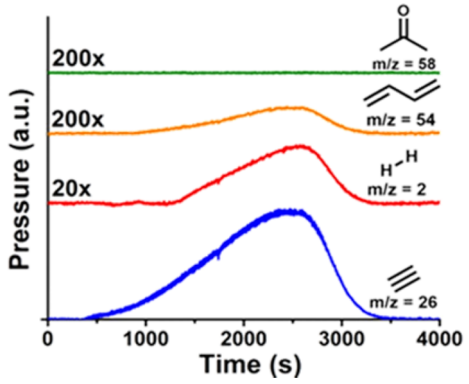

Figure 5. Pressure versus time graph for appearance of the vapor-phase products of the reduction of (-AlO_x)Pd(acac) with ethylene at 50 °C as assayed by mass spectrometry.

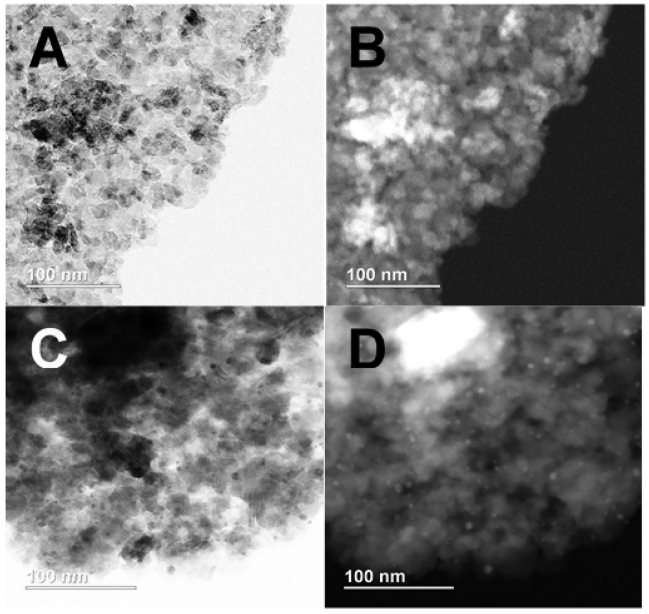

Figure 6. (A) BF-STEM image of (-AlO_x)Pd(acac) (no reduction). (B) HAADF-STEM image of (-AlO_x)Pd(acac) (no reduction). (C) Bright-field STEM image of (-AlO_x)Pd(acac) after reduction with 1-octene at 25 °C for 120 h. (D) HAADF-STEM image of (-AlO_x)Pd(acac) after reduction with 1-octene at 25 °C for 120 h.

DOI: 10.1021/acs.chemmater.7b04909
Chem. Mater. 2018, 30, 1032−1044

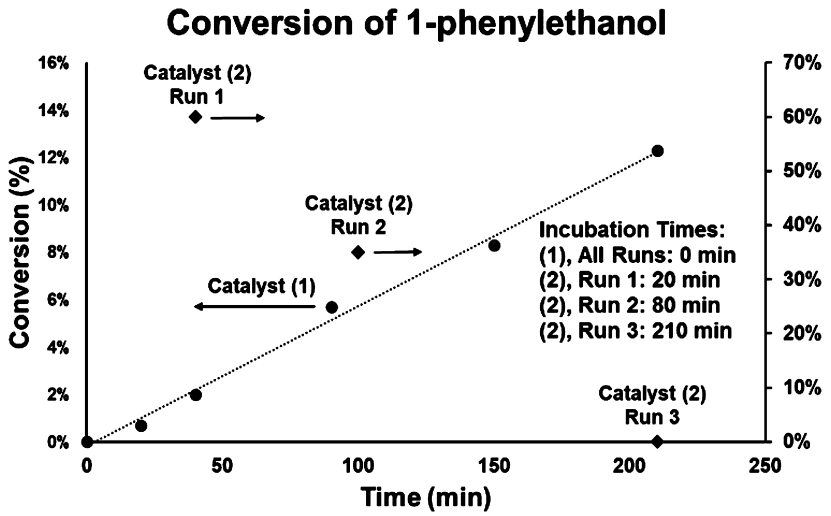

Figure 7. Catalytic oxidative conversion of 1-phenylethanol to acetophenone over Pd/Al_2O_3 prepared from the reduction of $(\text{-}AlO)_xPd(acac)$ with 1-octene at 25 °C (**1**), and a commercial 1% Pd/Al_2O_3 catalyst (**2**). Reaction conditions: 1 mmol 1-phenylethanol, 5 mL trifluorotoluene, 80 °C, under ambient air.

HAADF-STEM imaging modes, respectively. After the reduction with 1-octene, nanoparticles are observable by both BF- and HAADF-STEM (Figure 6C, D). The image sets in Figure 6A, B and Figure 6C, D were recorded at the same focal point and indicate the same alumina surface in both imaging modes.

Catalytic Oxidation of 1-Phenylethanol. The preparation of a Pd/Al_2O_3 catalyst in the absence of capping agents or surfactants is expected to yield Pd nanoparticles with chemically accessible surfaces. Accordingly, the performance of Pd/Al_2O_3 catalysts prepared via reduction of Pd/Al_2O_3 with 1-octene at 25 °C, for the catalytic oxidation of 1-phenylethanol was assessed (Figure 7). Aerobic oxidation of benzylic alcohol species has recently emerged as an attractive diagnostic reaction for novel Pd nanoparticle preparations due to the high activity and selectivity of typical supported Pd catalysts for such reactions.[71] In the present work, catalytic activity is obtained from the conversion of 1.0 mmol of 1-phenylethanol with the 0.1 mol % Pd catalyst at 80 °C under air in a batch reactor, using trifluorotoluene as the solvent. The conversion ratio is obtained from NMR analysis using an adamantane internal standard. Mass balance in these reactions is observed to be >95%, with >95% selectivity for the major product, acetophenone. These results are compared here to those obtained using a commercial catalyst (1% Pd supported γ-Al_2O_3, Sigma-Aldrich) (**2**; Figure 7). To accurately assess turnover frequencies (TOFs) per atom of accessible Pd^0, we measured the particle size of the commercial catalyst via HAADF-STEM. A count of 53 nanoparticles gave a mean particle diameter of 2.9 ± 0.5 nm. Further information on conditions, calculations, and quantification are presented in the Scheme S1, Figures S15−S17, and Tables S5 and S6. Results for catalyst **1** are provided as the average of three runs. Results for catalyst **2** are complicated by the observation that, in all cases, no reaction is observed until after a catalyst "incubation" period under reaction conditions. This incubation period varies from 20−210 min, and could not be eliminated by pretreating catalyst **2** under conventional conditions of 4 h calcination at 550 °C under flowing O_2, followed by reduction with 5% H_2/N_2 for 1 h. In contrast, no incubation period is observed for catalyst **1**.

The variable incubation time observed for catalyst **2** makes the comparison of TOFs for catalysts **1** and **2** problematic; therefore, three independent runs of catalyst **2** are presented in Figure 7. Catalyst **1** mediates the oxidation of 1-phenylethanol with a TOF of 216 ± 20 h^{-1} at 80 °C under ambient air (conversion <12.3%). The activity of catalyst **2** is estimated to be ∼540 h^{-1} from runs in which the catalyst performed adequately. The TOFs reported here are adjusted for the dispersion of the Pd^0 active species. Although commercial catalyst **2** exhibits approximately twice the rate of catalyst **1**, the high degree of variability in catalytic performance is undesirable, and at least one run yielded 0% conversion.

DISCUSSION

Surface Structure of $(\text{-}AlO_x)Pd(acac)$. The grafting reaction of $Pd(acac)_2$ is reasonably assumed to proceed via the elimination of an equivalent of acetylacetone rather than via a physisorption mechanism, evident from the limited reaction between the solution phase precursor and the support. Even in the presence of "excess" $Pd(acac)_2$, the maximum Pd loading achieved under the present chemisorption conditions is 0.2 wt %, yielding a Pd surface density of 0.2 Pd/nm^2. Extrapolating from the findings of van Veen et al.[51] and this laboratory,[53] this suggests that only certain, highly reactive hydroxyls on the γ-Al_2O_3 surface are capable of reacting protonolytically with $Pd(acac)_2$ at 25 °C. The stoichiometry of the reaction could not be determined via a titration method due to the strong adsorption of the free acetylacetone on γ-Al_2O_3 as determined via TPD-MS and DRIFTS, however, XPS, EXAFS, DRIFTS, and DNP SENS studies are consistent with the proposed $(\text{-}AlO_x)Pd(acac)$ surface complex structure (Chart 1 above).

The ^{13}C DNP SENS reveals an asymmetric surface complex, exhibiting two distinct ^{13}C signals for the methyl and carbonyl carbons of the acetylacetonato moiety. It is reasonable to assume that this asymmetry arises from interactions between one oxygen atom on the ligand, and either a surface hydroxyl or a surface Lewis acid site, as such interactions have been observed previously.[72] EXAFS reveals a Pd−O CN of ∼4, suggesting the species shown in Chart 1 to be the most likely geometry of the complex. The unique geometry of the surface complex appears to be critical in its reactivity with alkenes. In

DOI: 10.1021/acs.chemmater.7b04909
Chem. Mater. 2018, 30, 1032−1044

control experiments, the parent precursor $Pd(acac)_2$ could not be reduced with 1-octene at 25 °C, and isolated Pd^{2+} cations appear to be nonreducible under the present conditions (vide infra). These findings are consistent with previous literature reports.[73,74]

Reduction Process and Pd Nanoparticle Formation. Upon exposure to alkenes, (-AlO_x)Pd(acac) undergoes reduction (Figures 1–3) and Pd nanoparticles form on the alumina surface (Figures 6A–D). Deconvolution of the XPS ionization and fitting of the XANES spectrum yields quantitative information regarding the relative amounts of Pd^{2+} and Pd^0 (Figure 8). Both the XPS and XANES reveal that

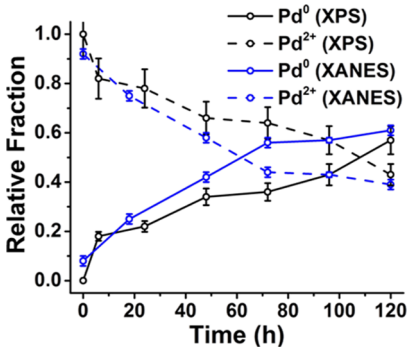

Figure 8. Relative fractions of Pd^{2+} and Pd^0 as a function of (-AlO_x)Pd(acac) reduction time with 1-octene.

the reaction of (-AlO_x)Pd(acac) with 1-octene is complete when ~60% of the Pd supported on the Al_2O_3 surface is reduced to Pd^0. This contrasts with NMR data (Figure 1B) that imply complete conversion of the surface (-AlO_x)Pd(acac) complex within 120 h, with no signals except surface-bound acetylacetone and decomposition products detected. Note that the Pd($3d_{5/2}$) peaks in the XPS spectrum of the parent (-AlO_x)Pd(acac) complex are very broad (fwhm Pd($3d_{5/2}$) = 3.4 eV) relative to the peaks for Pd^0 (fwhm Pd($3d_{5/2}$) = 2.3 eV) and molecular $Pd(acac)_2$ (fwhm Pd($3d_{5/2}$) = 2.3 eV). This phenomenon has been previously observed and assigned to highly dispersed Pd^{2+} species in close contact with an insulating support, (i.e., γ-Al_2O_3).[75] Other reports indicate that isolated Pd^{2+} cations do not participate in reduction reactions and nanoparticle formation, since they are stabilized by support interactions.[73,74,76] On this basis, it is reasonable to assume that two surface species are present after the reductive treatment – Pd^0 species present as nanoparticles, and isolated Pd^{2+} cations on the alumina surface which do not undergo reduction. Isolated Pd^{2+} cations do not contribute to the ^{13}C NMR signal, but do broaden the peaks in the Pd XPS spectrum.

After 120 h of (-AlO_x)Pd(acac) reduction with 1-octene, the EXAFS data indicate an average Pd···Pd CN of ~6 (Figure 3B, Figures S12 and S13, Table S4), too low to be consistent with the 4.3 nm particles observed via STEM (Figure 6). These results are, however, in good agreement with reports from the literature[77] and have previously been associated with the presence of very small (d < 6–8 Å) supported Pd clusters not observable by TEM.[78] An isolated Pd^{2+} cation has an effective Pd···Pd CN = 0, which skews the aggregate value toward a lower CN. Therefore, given that the present XPS, XANES, and EXAFS data for the sample treated with 1-octene at 25 °C for 120 h reveal that ~60% of the total Pd supported on the Al_2O_3 surface is present as Pd^0 and ~40% exists as isolated Pd^{2+} cations, either bound directly to the support or in very small clusters undetectable by STEM and DNP SENS, an average CN of 6 is fully expected. The possibility of a passivating Pd oxide layer on the nanoparticle surface cannot be entirely discounted; however, EXAFS evidence indicates a decreasing Pd–O coordination number as reduction progresses (from CN = 4.2 to CN = 1.7, Figure S13). As the expected Pd–O coordination number of PdO is CN = 4,[79] the EXAFS evidence suggests the majority of remaining Pd^{2+} species do not exist as Pd oxide.

Mechanism of (-AlO_x)Pd(acac) Reduction. To probe the reduction pathway of the well-defined surface complex, (-AlO_x)Pd(acac), the surface and gaseous reaction products were analyzed by DRIFTS and TPR-MS under ethylene at 50

Scheme 1. Proposed (-AlO_x)Pd(acac) Reaction with Ethylene Effecting Pd^{2+} → Pd^0 Reduction: (A) Ethylene Coordination to (-AlO_x)Pd(acac) and C–H Activation To Yield Pd-Alkenyl Intermediate 1; (B) Ethylene Insertion to Form a Bound Butenyl Fragment with Subsequent H-Elimination and H_2 Generation; (C) Direct β-Hydride Elimination from a Pd-Alkenyl To Yield Acetylene, Followed by Reductive Elimination, Generating an Equivalent of Acetylacetone and a Pd^0 Surface Species

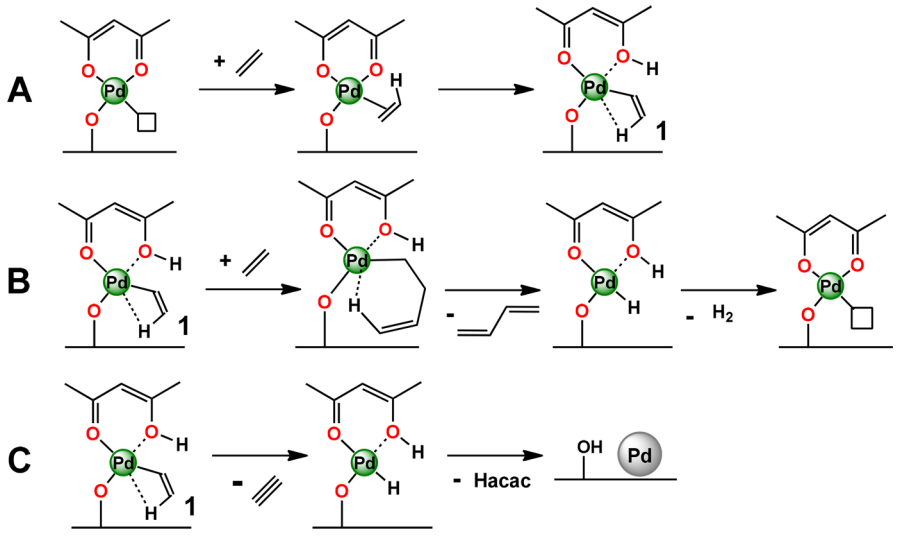

DOI: 10.1021/acs.chemmater.7b04909
Chem. Mater. 2018, 30, 1032–1044

°C. In the DRIFTS study, the difference spectrum taken after complete reduction of (-AlO_x)Pd(acac) with ethylene exhibits several significant features. The hydroxyl region of the DRIFTS spectrum (Figure 4A; absorbance mode) exhibits a broad negative band centered around 3641 cm^{-1}, indicating the consumption of surface hydroxyls during the reduction process. The hydrocarbon region of the spectrum (ca. 3000−2800 cm^{-1}) reveals no additional surface hydrocarbon species (Figure S3B), suggesting negligible transfer of ethylene to the surface. It is unclear whether hydroxyl consumption occurs via interaction with Pd nanoparticles or from protonolysis of the acac ligand by surface hydroxyl groups.[51] However, the lower-frequency region of the spectrum (Figure 4B) reveals that free acetylacetone species form after the reduction and remain stable on the alumina surface. The absence of new surface hydrocarbon species, particularly polyethylenes,[80] prompted further scrutiny of the gas-phase reaction products. The vapor-phase products detected by TPR-MS during reduction (Figure 5) are H_2, acetylene, and butadiene. The evolution of acetone was not observed at 50 °C, suggesting that direct decomposition of the acac-ligand is not involved in the reduction process. Acetylene and H_2 have been observed during the dehydrogenation of ethylene over metallic Pd.[70,81] This process is driven by the thermodynamics of coke coproduct formation, which is negligible here as verified by DRIFTS. In the present system, therefore, the formation of acetylene must be driven by the thermodynamically favorable sintering of reduced Pd^0 species into nanoparticles.[82,83] This also accounts for the surprising mobility of Pd^0 atoms on the γ-Al_2O_3 surface at such low temperatures. Interestingly, the production of H_2, acetylene, and butadiene ceases once the reduction process is complete (Figure 5), arguing that only (-AlO_x)Pd(acac) is active in the reaction, and neither the remaining Pd^{2+} cations nor the 4.3 nm nanoparticles are involved.

The sum of the data presented here suggests that reduction of (-AlO_x)Pd(acac) by ethylene proceeds first by activation of an ethylene C−H bond to form a Pd-alkenyl intermediate (Scheme 1). Although ethylene does not undergo polymerization under the present conditions, the presence of butadiene implicates a C−C bond-forming reaction in the overall reductive process. Pd^{2+} catalysts are known to be active for olefin dimerization and polymerization.[84−86] While the mechanism of polymerization is known to proceed via insertion of olefin into a Pd−C or Pd−H bond, the activation step is still under discussion.[87] Previous studies implicate electrophilic cleavage of olefinic C−H bonds rather than oxidative addition, a mechanistic scenario which maintains Pd in the 2+ oxidation state rather than invoking formal Pd^{2+}/Pd^{4+} redox cycles.[88] Recently, the heteroleptic activation of an ethylene C−H bond by the isolated Cr(II) sites of a catalyst supported on silica was reported,[47,89,90] leading to a metal-vinyl intermediate. The pathway proposed in Scheme 1 presents a possible reaction sequence accounting for formation of all observed products and reduction of Pd^{2+} to Pd^0, which would occur via reductive elimination from a Pd-alkenyl species as reported for other catalysts.[91−93]

An analogous mechanism is reasonable for 1-octene reduction in the liquid phase. Alternatively, Copéret et al. presented evidence for surface O atom site involvement in H atom transfer during alkene dehydrogenation;[94,95] this pathway may also be operative in the present system.

Mechanism of Pd Nanoparticle Formation. As the surface (-AlO_x)Pd(acac) complex decomposes to free Pd^0, nanoparticles are observed on the γ-Al_2O_3 surface via BF- and HAADF-STEM (Figure 6A−D, and Figures S4−S8). The presence of nanoparticles is furthermore confirmed by EDX (Figure S4). Interestingly, although XPS and XANES data (Figures 2 and 3A) indicate that the reduction is not instantaneous, the BF- and HAADF-STEM reveals that the particle size distribution of Pd nanoparticles remains invariant across the range from Pd^0 fractions of 20−60%. Representative statistics on the Pd nanoparticle sizes at different reaction times are presented in Figures S10 and S11 and Tables S2 and S3. Two dominant models for nanoparticle nucleation and growth on support surfaces are Ostwald ripening (OR) and particle migration/coalescence (PMC).[96,97] The kinetics of particle growth can be considered as a function of the metal−support interface energetics (interface-controlled regime) and the diffusion across the support surface (diffusion-controlled regime).[98] In each case, the specific energetics are likely related to the chemical identity of the mobile Pd "monomer," a factor expected to change with the chemical reductant.

The profile of the particle size distribution is typically an indicator of the dominant nucleation and growth mechanism. In the case of the diffusion-controlled OR models, the particle size distributions are expected to be symmetric or skewed toward particles of smaller size.[98−100] In contrast, a mechanism dominated by PMC is expected to show significant skew toward larger sizes.[101,102] Note that smaller, higher energy particles (<3 nm) are anticipated to be highly mobile, leading to a metastable distribution of medium-sized particles (3−10 nm) that sinter at a slower rate.[96] As the particle size increases, OR dominates the sintering mechanism.[103] Note also that PMC is more relevant at elevated temperatures (>500 °C). Based on these guidelines and considering the narrow distribution of observed particles in the present materials, it is most likely that the initial sintering of Pd particles to the 4.3 nm mean diameter is rapid and may occur by a combination of PMC and OR mechanisms; however, once this mean diameter is reached, PMC effects appear to be negligible, while further sintering via OR is minimized by the low temperatures and overall low surface density of Pd centers. The narrow range of Pd nanoparticle sizes formed here therefore suggests that the initial parent (-AlO_x)Pd(acac) complex is well-dispersed over the alumina surface, as surface complexes "clustered" in particular areas would be expected to yield larger particles upon reduction, in accordance with an OR mechanism. From this it is also reasonable to infer that the stability of the 4.3 nm particles is likely due to rapid depletion of local concentrations of the mobile Pd^0 "monomer" as nanoparticles aggregate; the resulting spatial isolation likely reduces the tendency of the particles to sinter via the OR mechanism.

Catalytic Relevance of Pd Nanoparticle Formation via Alkene Reduction. Preparation of supported Pd nanoparticles from (-AlO_x)Pd(acac) and 1-octene yields catalyst **1**, which is competent for the aerobic oxidation of 1-phenylethanol to acetophenone, as shown in Figure 7 (see also Figures S15−S17). In contrast to commercial catalyst **2**, catalyst **1** exhibits immediate activity under ambient conditions with no incubation period. This finding suggests that not only is the Pd surface in catalyst **1** of sufficient accessibility for catalysis, but that the active Pd^0 species in **1** is formed directly by the 1-octene reduction process. In contrast, the Pd^0 species present in commercial catalyst **2** appears to be a "pre-catalyst" to an unknown Pd^0 active species, despite the presence of 2.9 nm Pd^0 nanoparticles in the as-prepared catalyst. This is consistent with

DOI: 10.1021/acs.chemmater.7b04909
Chem. Mater. 2018, 30, 1032−1044

literature reports of supported Pd catalyst evolution under reaction conditions,[104] particularly in aerobic oxidation processes.[105,106] Previously, this phenomenon was ascribed to complex surface interactions between the substrate, oxidant, and the oxidation−reduction cycle of Pd^0/Pd^{2+} species during reaction.[107] Although the exact distribution of Pd^{2+} cations relative to Pd^0 nanoparticles is unknown, literature reports[107,108] suggest that proximity of Pd^0 and Pd^{2+} species on the surface of catalyst **1** may contribute to its immediate activity in aerobic oxidation in contrast to the more reduced commercial catalyst.

In optimum runs, commercial catalyst **2** exhibits approximately twice the activity of catalyst **1** for 1-phenylethanol to acetophenone oxidation. The enhanced activity of **2** is not unexpected, as the particle size is smaller than in **1**, 2.9 nm versus 4.3 nm, respectively. It is well-known that smaller Pd nanoparticles exhibit higher activity, particularly in alcohol oxidation.[109,110] The variability in the performance of catalyst **2**, along with its failure to convert any substrate in at least one run, however, demonstrates the attraction of the well-defined system presented here. The reduction of $(\text{-AlO})_x$Pd(acac) with alkenes at mild temperatures yields a "true" Pd^0 catalyst that exhibits immediate activity in aerobic oxidation.

■ CONCLUSIONS

An approach for preparing single-site, well-defined Pd surface complexes of the form (-AlO_x)Pd(acac) from a simple grafting reaction of $Pd(acac)_2$ on γ-Al_2O_3 is presented. Exposure of this Pd^{2+}complex to alkenes results in facile reduction to a Pd^0 species, which agglomerates to form 4.3 ± 0.6 nm nanoparticles. The present results suggest that a combination of surface organometallic chemistry and mild reduction conditions can be used to prepare controlled dispersions of nanoparticles on high surface area supports. In comparison to a commercial Pd/Al_2O_3 catalyst, the catalyst obtained by (-AlO_x)Pd(acac) reduction with 1-octene exhibits immediate activity in the aerobic oxidation of 1-phenylethanol to acetophenone with no incubation period, confirming the clean nature of the catalytic surface. The level of mechanistic detail regarding the reduction and nanoparticle formation processes is facilitated by the single-site approach. Such a study affords better understanding of the complex mechanisms underlying the preparation of supported metal catalysts on high surface area refractory oxides.

■ MATERIAL AND METHODS

Where indicated, air-sensitive manipulations were carried out using standard Schlenk line glassware and techniques under an N_2 atmosphere. Ar (UHP) and He (UHP) were purchased from Airgas and further purified through an entrained drying column. Oxygen (UHP) and regen gas (5% H_2/N_2) were purchased from Airgas and used directly without further purification. Palladium(II) acetylacetonate (99%) was purchased from Strem Chemicals and used without further purification. The reagent 1-octene (98%) was purchased from Sigma-Aldrich and further purified by distillation from sodium under an atmosphere of N_2; after distillation, the 1-octene was stored under N_2 in the dark at 2−8 °C. Ethylene (UHP, 99.995%) was purchased from Airgas and used without further purification. Anhydrous toluene and pentanes were purchased from Sigma-Aldrich and further purified on activated alumina columns. Hexanes and $CDCl_3$ were purchased from Sigma-Aldrich and used without further purification. The substrate 1-phenylethanol (98%) was purchased from Sigma-Aldrich and used without further purification. Commercial, 1% Pd/γ-Al_2O_3 was purchased from Sigma-Aldrich. Phase-pure γ-Al_2O_3 (99.997% purity metals basis, 60 m^2/g surface area, < 3 μm particle size) was purchased from Alfa-Aesar and calcined at 550 °C in flowing O_2 for 18 h prior to use. No surface contaminants were detected by XPS. DRIFTS spectra of adsorbed ethylene and reduced Pd/Al_2O_3 were measured in the CleanCat core facility at Northwestern on a Nicolet 6700 spectrophotometer equipped with a gas flow cell and a sample heater. DNP-enhanced solid-state NMR spectra were obtained at the Ames Laboratory using a Bruker DNP-MAS NMR spectrometer equipped with a 264 GHz gyrotron and a 3.2 mm low-temperature MAS probe. X-ray photoelectron spectra were measured in the Keck core facility at Northwestern with a Thermo Scientific ESCALAB 250 Xi spectrophotometer equipped with an electron flood gun and an Al K-α source. Temperature-programmed reaction mass-spectrometry (TPR-MS) experiments were performed with an AMI-200 TPR apparatus and measured with a Stanford Research Systems UGA100 Universal Gas Analyzer. TEM and EDX measurements were taken on a Hitachi HD-2300 Dual EDS Cryo STEM. XAS measurements were completed at beamline 5BM-D at the Advanced Photon Source (APS) at Argonne National Laboratory. The Pd atom oxidation state(s) and local atomic coordination structure were analyzed by XANES and EXAFS, respectively. These ex situ (open air) XANES and EXAFS measurements of the Pd/Al_2O_3 samples were carried out around the Pd K-edge (24.4 keV). The powder Pd/Al_2O_3 samples were prepressed (12 mm in diameter and ∼0.5 mm in thickness) and measured in fluorescence mode. Quantitative measurements of Pd loadings were obtained by ICP-AES from Galbraith Laboratories, Inc.

Synthesis of (-AlO_x)Pd(acac). Prior to reaction, all glassware was dried at 150 °C overnight and cooled under dynamic vacuum. Calcined γ-Al_2O_3 (5.0 g) was treated similarly and held under an atmosphere of N_2 after cooling. In a separate flask, 0.36 g $Pd(acac)_2$ (1.1 mmol, 2.5 wt % Pd) was dissolved in ca. 25 mL of anhydrous toluene. The golden solution was cannulated onto the γ-Al_2O_3 under N_2 and the resulting suspension stirred for 18 h at 25 °C. The suspension was allowed to settle and the golden mother liquor cannula filtered from the solid. The solid was then washed twice with 25 mL of anhydrous toluene under N_2, filtering off the wash liquid in the manner previously described. When the wash was no longer colored, the solid was suspended in hexanes and vacuum filtered in open air. The resulting beige solid was further washed with hexanes to remove excess toluene and dried under dynamic vacuum at 25 °C overnight. After preparation, the solid could be stored under ambient conditions indefinitely with no observable degradation of the (-AlO_x)Pd(acac) surface complex. ICP analysis of several preparations indicated the Pd loading to be 0.20 ± 0.01% Pd.

Reduction of (-AlO_x)Pd(acac). Liquid-phase Reduction with 1-Octene. In a typical reduction experiment, an oven-dried, vacuum-cooled flask was charged with 0.60 g of (-AlO_x)Pd(acac) (0.20 wt % Pd) under a stream of N_2. The flask was evacuated and recharged with N_2 thrice. Subsequently, 10 mL of 1-octene was added to the solid via syringe, and the resulting suspension was stirred for a set length of time. To terminate the reaction, the solid was immediately vacuum-filtered in open air, followed by extensive washing with hexanes. Reduced samples changed color from beige to gray. After reduction, the sample was dried under dynamic vacuum at 25 °C overnight prior to further experiments.

Liquid or Solventless Reduction with Ethylene. An oven-dried, vacuum-cooled pressure vessel was charged with 0.6 g of (-AlO_x)Pd(acac) (0.2 wt % Pd). The solid was either suspended in ca. 10 mL of pentanes or left dry in the vessel. The vessel was evacuated to 10^{-5} Torr (the pentanes suspension was first cooled to −196 °C in a liquid nitrogen flask to prevent evacuation of the pentanes) and pressurized with 1 atm of ethylene (99.995%). The reaction was then stirred overnight before the vessel was evacuated and the solid material recovered (by filtration in the case of the pentanes suspension). Reduced material was dried under dynamic vacuum at 25 °C overnight before use in further experiments.

Catalytic Reactions. Catalytic experiments were performed using either a Pd/Al_2O_3 catalyst (0.2 wt % Pd) prepared by reduction of (-AlO_x)Pd(acac) for 120 h with 1-octene at 25 °C, or with a commercially obtained 1% Pd/γ-Al_2O_3 catalyst (Sigma-Aldrich). The mean Pd particle diameter of the commercial catalyst was determined

DOI: 10.1021/acs.chemmater.7b04909
Chem. Mater. 2018, 30, 1032−1044

from HAADF-STEM to be 2.9 nm (SD = 0.5 nm), while the mean Pd particle diameter for our catalyst was determined to be 4.3 nm (SD = 0.6 nm) by BF-STEM.

In a typical experiment, 1-phenylethanol (Sigma, 98%, 1 mmol, 0.12 mL) and the catalyst (0.05 g) were loaded under air into a 25 mL flask with Morton indentations, following by the addition of $PhCF_3$ (5.0 mL) as the solvent. This flask was then interfaced to a reflux condenser, and the mixture was rapidly stirred and placed in a temperature-controlled oil bath at 80 °C. NMR aliquots of the reaction solution were withdrawn at periodic intervals during the reaction and analyzed using adamantane (0.25 mmol, 0.034 g) as the internal standard. Conversion and selectivity (based on the loss of reactant) at differential conversions were difficult to obtain without significant error due to significant incubation times (40−120 min) displayed by the commercial catalyst. Mass balance was typically observed to be >95% and acetophenone was the only detectable product. Turnover frequencies were calculated on a (mol product)/(mol surface Pd^0) basis, adjusted for the particle sizes determined by HAADF-STEM (see the Supporting Information for more details).

In an effort to eliminate the incubation period observed for the commercial Pd/Al_2O_3 catalyst, the material was calcined (4 h, flowing O_2, 550 °C) and reduced (1 h, 300 °C, 5% H_2/N_2). These pretreatments had no impact on the incubation time. Results for the homemade variant are reported as the average of 3 runs. Results for the commercial catalyst are reported as the best-run results.

XPS Measurements. A sample of powder was packed tightly onto double-sided copper tape attached to a stainless steel sample tray. The sample tray was outgassed in the sample entry chamber until a vacuum of at least 2×10^{-5} Torr was obtained, typically requiring 30 min. The sample tray was then admitted to the UHV chamber and the electron flood gun turned on to compensate for charge. The sample was further allowed to outgas in the UHV chamber until stable vacuum was obtained, typically on the order of 8×10^{-8} Torr. Spectra were measured in the CAE mode with 50 50 scans apiece at a pass energy of 20 eV. The resulting spectra were background-subtracted and peak-fitted according to standard software techniques. Before deposition, no species other than C, Al, and O were detected on the catalyst surface. After deposition, no species other than C, Al, O, and Pd were detected on the catalyst surface. To compensate for charging effects the binding energies of all observed peaks were corrected by setting the adventitious carbon peak to 285.0 eV.

DRIFTS Measurements. In a typical environmental DRIFTS measurement, the powder was tightly packed into a sample cup affixed atop a sample heater. The heater was regulated with a flow of room-temperature water pumped through a peristaltic pump. The sample cup was heated to 50 °C and allowed to equilibrate for several hours under argon until no further shift in the background spectrum was observed. The background spectrum was obtained and the gas flow was switched to ethylene. The progress of reduction was tracked over the course of 8 h by acquiring spectra at progressive time points until no further change was observed in the difference spectrum. After completion of the reduction reaction, the chamber was purged with Ar and the final difference spectrum acquired under an inert atmosphere.

^{13}C DNP SENS. All DNP NMR experiments were performed using a commercial 400 MHz Bruker DNP-MAS NMR spectrometer. Samples of (-AlO_x)Pd(acac) at different reduction stages were impregnated with a 10 mM water solution of the biradical AMUPol and immediately packed into 3.2 mm sapphire rotors. The samples were sealed using a Teflon plug and spun at 25 °C using a Vespel cap to symmetrically distribute the studied materials in the MAS rotor prior to performing the low-temperature experiments. The Vespel cap was exchanged for a zirconia cap for the low-temperature experiments. All ^{13}C CPMAS experiments were performed using a 2.35 μs ^1H excitation pulse, a 3 ms CP contact time, and SPINAL-64 ^1H decoupling. The recycle delay was set to 7 s and a total of 2048 scans were accumulated under continuous wave microwave irradiation at around 105 K.

TPR-MS and TPD-MS. A sample of (-AlO_x)Pd(acac) (typically 0.50 g) was placed atop a packed quartz wool bed in a quartz U-tube and affixed in the AMI-200 TPR apparatus. The effluent from the gas stream was connected to a Universal Gas Analyzer for real-time mass spectrometric analysis of the reaction products. The gas stream was switched from He to ethylene (99.995%) and pure ethylene flowed through the powder. Reaction products were first measured via an analog scan from 1 to 100 amu to determine which masses evolved with time; reaction products were then confirmed via a pressure versus time (PVT) measurement over the course of ca. 1 h. After completion of the experiment, the powder bed was heated at a ramp rate of 5 °C/min in a flow of 10 sccm He to determine if any reaction products were adsorbed on the powder; only acetone, the decomposition product of alumina-bound acetylacetone, was observed, confirming other observations that the products of the reaction are the expected gaseous products. TPD-MS after the reaction was performed by ramping the temperature at from 50−550 °C in a flow of 10 sccm He. Products from 1−100 m/z were detected via analog scans at a rate of 1 scan/6 s.

STEM and EDX Measurements. TEM images of the Pd nanoparticles on γ-Al_2O_3 were acquired using a Hitatchi HD-2300A STEM under phase contrast imaging at an accelerating voltage of 200 kV. The Hitachi HD-2300A STEM is equipped with an ultrasensitive dual energy dispersive X-ray (EDX) spectrometer system that was used to obtain elemental analysis of the samples. Samples for TEM and EDX were prepared by dropping a methanol dispersion of each material onto a lacey carbon-coated copper grid and allowing the solvent to evaporate.

EXAFS and XANES Measurements. The fractions of Pd^{2+} and Pd^0 were obtained from linear combination fitting analysis. XANES spectra of $Pd(acac)_2$ (Pd^{2+}) and Pd foil (Pd^0) were used as the standards in the fitting analysis. The fitting range was −20−30 eV with respect to the Pd K-edge. The coordination numbers (N) of Pd−Pd and Pd−O bonds, Pd−Pd and Pd−O bond distances (r), and Debye−Waller factors (σ), were obtained by a least-squares fitting in R-space between 1−3.5 Å of the k^2-weighted Fourier transformed EXAFS data (k = 2.5−11 $Å^{-1}$). Photoelectron scattering paths used in the fitting were based on the first nearest neighbors of Pd in fcc Pd (Pd−Pd) and tetragonal PdO (Pd−O). Data processing was completed with the ATHENA and ARTEMIS software packages.[111]

■ ASSOCIATED CONTENT

Supporting Information

The Supporting Information is available free of charge on the ACS Publications website at DOI: 10.1021/acs.chemmater.7b04909.

Deconvoluted XPS spectra and XPS parameters, additional DNP SENS data, additional TEM images and particle counts, additional DRIFTS data, additional XAS Spectra, catalytic parameters (PDF)

■ AUTHOR INFORMATION

Corresponding Authors

*E-mail: pstair@northwestern.edu (P.C.S.).
*E-mail: t-marks@northwestern.edu (T.M.).
*E-mail: delferro@anl.gov (M.D.).

ORCID

Cassandra L. Whitford: 0000-0002-8223-7516
Marek Pruski: 0000-0001-7800-5336
Michael J. Bedzyk: 0000-0002-1026-4558
Massimiliano Delferro: 0000-0002-4443-165X
Tobin J. Marks: 0000-0001-8771-0141

Present Address

#M.D. is currently at Chemical Sciences & Engineering Division, Argonne National Laboratory, Lemont, Illinois 60439, USA

DOI: 10.1021/acs.chemmater.7b04909
Chem. Mater. 2018, 30, 1032−1044

Author Contributions

The manuscript was written through contributions of all authors. All authors have given approval to the final version of the manuscript.

Funding

This material is based upon work supported by the U.S. Department of Energy, Office of Science, Office of Basic Energy Sciences, grant DE-FG02-03ER154757. Support for C.W. is through an NSF grant, DMR-1334928. Support for F.P. is through a Spedding Fellowship, which is funded by the Ames Laboratory's LDRD program. Ames Laboratory is operated for the U.S. Department of Energy by Iowa State University grant number DE-AC02-07CH11358. F.P. thanks the National Sciences and Engineering Research Council of Canada (NSERC) and the government of Canada for a Banting Fellowship. This work made use of the (EPIC and Keck-II) facilities of the NU*ANCE* Center at Northwestern University, which has received support from the Soft and Hybrid Nanotechnology Experimental (SHyNE) Resource (NSF NNCI-1542205); the MRSEC program (NSF DMR-1121262) at the Materials Research Center; the International Institute for Nanotechnology (IIN); the Keck Foundation; and the State of Illinois, through the IIN. X-ray measurements were performed at Advanced Photon Source Sector 5 (DND-CAT) located at Argonne National Laboratory, which is supported by the U.S. Department of Energy, Office of Science, and Office of Basic Energy Sciences, under Contract DE-AC02-06CH11357. DND-CAT is supported by through E. I. duPont de Nemours & Co., Northwestern University, Dow Chemical Co., the State of Illinois through the Department of Commerce and the Board of Education (HECA), and the US National Science Foundation. The CleanCat Core facility acknowledges funding from the U.S. Department of Energy (DE-FG02-03ER15457) used for the purchase of the Nicolet 6700 FT-IR, Harrick DRIFTS accessory, and Altamira AMI- 200.

Notes

The authors declare no competing financial interest.

■ ACKNOWLEDGMENTS

The authors acknowledge Dr. J. Tan for helpful discussions and comments.

■ REFERENCES

(1) White, R. J.; Luque, R.; Budarin, V. L.; Clark, J. H.; Macquarrie, D. J. Supported metal nanoparticles on porous materials. Methods and applications. *Chem. Soc. Rev.* **2009**, *38* (2), 481−494.

(2) Astruc, D.; Lu, F.; Aranzaes, J. R. Nanoparticles as Recyclable Catalysts: The Frontier between Homogeneous and Heterogeneous Catalysis. *Angew. Chem., Int. Ed.* **2005**, *44* (48), 7852−7872.

(3) Hayden, B. E.; Pletcher, D.; Rendall, M. E.; Suchsland, J.-P. CO Oxidation on Gold in Acidic Environments: Particle Size and Substrate Effects. *J. Phys. Chem. C* **2007**, *111* (45), 17044−17051.

(4) Gunter, P. L. J.; Niemantsverdriet, J. W.; Ribeiro, F. H.; Somorjai, G. A. Surface Science Approach to Modeling Supported Catalysts. *Catal. Rev.: Sci. Eng.* **1997**, *39* (1−2), 77−168.

(5) Goodman, D. W. Model Studies in Catalysis Using Surface Science Probes. *Chem. Rev.* **1995**, *95* (3), 523−536.

(6) Quek, X.-Y.; Pestman, R.; van Santen, R. A.; Hensen, E. J. M. Structure sensitivity in the ruthenium nanoparticle catalyzed aqueous-phase Fischer−Tropsch reaction. *Catal. Sci. Technol.* **2014**, *4* (10), 3510−3523.

(7) Michalak, W. D.; Krier, J. M.; Komvopoulos, K.; Somorjai, G. A. Structure Sensitivity in Pt Nanoparticle Catalysts for Hydrogenation of 1,3-Butadiene: In Situ Study of Reaction Intermediates Using SFG Vibrational Spectroscopy. *J. Phys. Chem. C* **2013**, *117* (4), 1809−1817.

(8) Somorjai, G. A.; Carrazza, J. Structure sensitivity of catalytic reactions. *Ind. Eng. Chem. Fundam.* **1986**, *25* (1), 63−69.

(9) Campbell, C. T. The Energetics of Supported Metal Nanoparticles: Relationships to Sintering Rates and Catalytic Activity. *Acc. Chem. Res.* **2013**, *46* (8), 1712−1719.

(10) Häkkinen, H.; Abbet, S.; Sanchez, A.; Heiz, U.; Landman, U. Structural, Electronic, and Impurity-Doping Effects in Nanoscale Chemistry: Supported Gold Nanoclusters. *Angew. Chem., Int. Ed.* **2003**, *42* (11), 1297−1300.

(11) Valden, M.; Lai, X.; Goodman, D. W. Onset of Catalytic Activity of Gold Clusters on Titania with the Appearance of Nonmetallic Properties. *Science* **1998**, *281* (5383), 1647−1650.

(12) Rodriguez, J. A.; Liu, P.; Wang, X.; Wen, W.; Hanson, J.; Hrbek, J.; Pérez, M.; Evans, J. Water-gas shift activity of Cu surfaces and Cu nanoparticles supported on metal oxides. *Catal. Today* **2009**, *143* (1−2), 45−50.

(13) Farmer, J. A.; Campbell, C. T. Ceria Maintains Smaller Metal Catalyst Particles by Strong Metal-Support Bonding. *Science* **2010**, *329* (5994), 933−936.

(14) Campbell, C. T.; Sellers, J. R. V. Anchored metal nanoparticles: Effects of support and size on their energy, sintering resistance and reactivity. *Faraday Discuss.* **2013**, *162* (0), 9−30.

(15) Hayden, B. E.; Pletcher, D.; Suchsland, J.-P.; Williams, L. J. The influence of support and particle size on the platinum catalysed oxygen reduction reaction. *Phys. Chem. Chem. Phys.* **2009**, *11* (40), 9141−9148.

(16) Heiz, U.; Bullock, E. L. Fundamental aspects of catalysis on supported metal clusters. *J. Mater. Chem.* **2004**, *14* (4), 564−577.

(17) Prieto, G.; Zečević, J.; Friedrich, H.; de Jong, K. P.; de Jongh, P. E. Towards stable catalysts by controlling collective properties of supported metal nanoparticles. *Nat. Mater.* **2013**, *12* (1), 34−39.

(18) Karim, A. M.; Al Hasan, N.; Ivanov, S.; Siefert, S.; Kelly, R. T.; Hallfors, N. G.; Benavidez, A.; Kovarik, L.; Jenkins, A.; Winans, R. E.; Datye, A. K. Synthesis of 1 nm Pd Nanoparticles in a Microfluidic Reactor: Insights from in Situ X-ray Absorption Fine Structure Spectroscopy and Small-Angle X-ray Scattering. *J. Phys. Chem. C* **2015**, *119* (23), 13257−13267.

(19) Huang, C.-C.; Lai, W.-C.; Tsai, C.-Y.; Yang, C.-H.; Yeh, C.-S. Reversible Synthesis of Sub-10 nm Spherical and Icosahedral Gold Nanoparticles from a Covalent $Au(CN)_2-$ Precursor and Recycling of Cyanide to form Ferric Ferrocyanide for Cell Staining. *Chem. - Eur. J.* **2012**, *18* (13), 4107−4114.

(20) Liz-Marzán, L. M.; Giersig, M.; Mulvaney, P. Synthesis of Nanosized Gold−Silica Core−Shell Particles. *Langmuir* **1996**, *12* (18), 4329−4335.

(21) Anderson, J. A.; Garcia, M. F. *Supported Metals in Catalysis*; World Scientific: Singapore, 2011; Vol. *11*.

(22) Xin, H. L.; Mundy, J. A.; Liu, Z.; Cabezas, R.; Hovden, R.; Kourkoutis, L. F.; Zhang, J.; Subramanian, N. P.; Makharia, R.; Wagner, F. T.; Muller, D. A. Atomic-Resolution Spectroscopic Imaging of Ensembles of Nanocatalyst Particles Across the Life of a Fuel Cell. *Nano Lett.* **2012**, *12* (1), 490−497.

(23) Newton, M. A.; Belver-Coldeira, C.; Martinez-Arias, A.; Fernandez-Garcia, M. Dynamic in situ observation of rapid size and shape change of supported Pd nanoparticles during CO/NO cycling. *Nat. Mater.* **2007**, *6* (7), 528−532.

(24) Campbell, C. T.; Parker, S. C.; Starr, D. E. The Effect of Size-Dependent Nanoparticle Energetics on Catalyst Sintering. *Science* **2002**, *298* (5594), 811−814.

(25) Park, J.; Aliaga, C.; Renzas, J. R.; Lee, H.; Somorjai, G. The Role of Organic Capping Layers of Platinum Nanoparticles in Catalytic Activity of CO Oxidation. *Catal. Lett.* **2009**, *129* (1−2), 1−6.

(26) Lu, J.; Fu, B.; Kung, M. C.; Xiao, G.; Elam, J. W.; Kung, H. H.; Stair, P. C. Coking- and Sintering-Resistant Palladium Catalysts Achieved Through Atomic Layer Deposition. *Science* **2012**, *335* (6073), 1205−1208.

DOI: 10.1021/acs.chemmater.7b04909
Chem. Mater. 2018, 30, 1032−1044

(27) O'Neill, B. J.; Sener, C.; Jackson, D. H. K.; Kuech, T. F.; Dumesic, J. A. Control of Thickness and Chemical Properties of Atomic Layer Deposition Overcoats for Stabilizing Cu/γ-Al2O3 Catalysts. *ChemSusChem* **2014**, *7* (12), 3247−3251.
(28) You, H.; Yang, S.; Ding, B.; Yang, H. Synthesis of colloidal metal and metal alloy nanoparticles for electrochemical energy applications. *Chem. Soc. Rev.* **2013**, *42* (7), 2880−2904.
(29) Cookson, J. The Preparation of Palladium Nanoparticles. *Platinum Met. Rev.* **2012**, *56* (2), 83−98.
(30) Mazumder, V.; Sun, S. Oleylamine-Mediated Synthesis of Pd Nanoparticles for Catalytic Formic Acid Oxidation. *J. Am. Chem. Soc.* **2009**, *131* (13), 4588−4589.
(31) Wang, Y.; Yang, H. Oleic acid as the capping agent in the synthesis of noble metal nanoparticles in imidazolium-based ionic liquids. *Chem. Commun.* **2006**, 2545−2547.
(32) Lidor-Shalev, O.; Zitoun, D. Reaction mechanism of ″amine-borane route″ towards Sn, Ni, Pd, Pt nanoparticles. *RSC Adv.* **2014**, *4* (109), 63603−63610.
(33) Wu, Z. G.; Munoz, M.; Montero, O. The synthesis of nickel nanoparticles by hydrazine reduction. *Adv. Powder Technol.* **2010**, *21* (2), 165−168.
(34) Bondi, J. F.; Oyler, K. D.; Ke, X.; Schiffer, P.; Schaak, R. E. Chemical Synthesis of Air-Stable Manganese Nanoparticles. *J. Am. Chem. Soc.* **2009**, *131* (26), 9144−9145.
(35) Chen, Y.; Liew, K. Y.; Li, J. Size-controlled synthesis of Ru nanoparticles by ethylene glycol reduction. *Mater. Lett.* **2008**, *62* (6−7), 1018−1021.
(36) Li, D.; Wang, C.; Tripkovic, D.; Sun, S.; Markovic, N. M.; Stamenkovic, V. R. Surfactant Removal for Colloidal Nanoparticles from Solution Synthesis: The Effect on Catalytic Performance. *ACS Catal.* **2012**, *2* (7), 1358−1362.
(37) Kim, C.; Lee, H. Change in the catalytic reactivity of Pt nanocubes in the presence of different surface-capping agents. *Catal. Commun.* **2009**, *10* (9), 1305−1309.
(38) Lu, J.; Stair, P. C. Nano/Subnanometer Pd Nanoparticles on Oxide Supports Synthesized by AB-type and Low-Temperature ABC-type Atomic Layer Deposition: Growth and Morphology. *Langmuir* **2010**, *26* (21), 16486−16495.
(39) Goldstein, D. N.; George, S. M. Surface poisoning in the nucleation and growth of palladium atomic layer deposition with $Pd(hfac)_2$ and formalin. *Thin Solid Films* **2011**, *519* (16), 5339−5347.
(40) Gharachorlou, A.; Detwiler, M. D.; Nartova, A. V.; Lei, Y.; Lu, J.; Elam, J. W.; Delgass, W. N.; Ribeiro, F. H.; Zemlyanov, D. Y. Palladium Nanoparticle Formation on TiO_2(110) by Thermal Decomposition of Palladium(II) Hexafluoroacetylacetonate. *ACS Appl. Mater. Interfaces* **2014**, *6* (16), 14702−14711.
(41) Costa, N. J. S.; Rossi, L. M. Synthesis of supported metal nanoparticle catalysts using ligand assisted methods. *Nanoscale* **2012**, *4* (19), 5826−5834.
(42) Fujdala, K. L.; Drake, I. J.; Bell, A. T.; Tilley, T. D. Atomic Level Control over Surface Species via a Molecular Precursor Approach: Isolated Cu(I) Sites and Cu Nanoparticles Supported on Mesoporous Silica. *J. Am. Chem. Soc.* **2004**, *126* (35), 10864−10866.
(43) Sohn, H.; Camacho-Bunquin, J.; Langeslay, R. R.; Ignacio-de Leon, P. A.; Niklas, J.; Poluektov, O. G.; Liu, C.; Connell, J. G.; Yang, D.; Kropf, J.; Kim, H.; Stair, P. C.; Ferrandon, M.; Delferro, M. Isolated, Well-Defined Organovanadium(III) on Silica: Single-Site Catalyst for Hydrogenation of Alkenes and Alkynes. *Chem. Commun.* **2017**, *53* (53), 7325−7328.
(44) Klet, R. C.; Tussupbayev, S.; Borycz, J.; Gallagher, J. R.; Stalzer, M. M.; Miller, J. T.; Gagliardi, L.; Hupp, J. T.; Marks, T. J.; Cramer, C. J.; Delferro, M.; Farha, O. K. Single-Site Organozirconium Catalyst Embedded in a Metal−Organic Framework. *J. Am. Chem. Soc.* **2015**, *137*, 15680−15683.
(45) Gu, W.; Stalzer, M. M.; Nicholas, C. P.; Bhattacharyya, A.; Motta, A.; Gallagher, J. R.; Zhang, G.; Miller, J. T.; Kobayashi, T.; Pruski, M.; Delferro, M.; Marks, T. J. Benzene Selectivity in Competitive Arene Hydrogenation: Effects of Single-Site Catalyst··· Acidic Oxide Surface Binding Geometry. *J. Am. Chem. Soc.* **2015**, *137* (21), 6770−6780.
(46) Williams, L. A.; Guo, N.; Motta, A.; Delferro, M.; Fragala, I. L.; Miller, J. T.; Marks, T. J. Surface Structural-Chemical Characterization of a Single-Site D(0) Heterogeneous Arene Hydrogenation Catalyst Having 100% Active Sites. *Proc. Natl. Acad. Sci. U. S. A.* **2013**, *110* (2), 413−418.
(47) Coperet, C.; Comas-Vives, A.; Conley, M. P.; Estes, D. P.; Fedorov, A.; Mougel, V.; Nagae, H.; Nunez-Zarur, F.; Zhizhko, P. A. Surface Organometallic and Coordination Chemistry toward Single-Site Heterogeneous Catalysts: Strategies, Methods, Structures, and Activities. *Chem. Rev.* **2016**, *116* (2), 323−421.
(48) Fedorov, A.; Liu, H.-J.; Lo, H.-K.; Copéret, C. Silica-Supported Cu Nanoparticle Catalysts for Alkyne Semihydrogenation: Effect of Ligands on Rates and Selectivity. *J. Am. Chem. Soc.* **2016**, *138* (50), 16502−16507.
(49) Chen, F.; Kreyenschulte, C.; Radnik, J.; Lund, H.; Surkus, A.-E.; Junge, K.; Beller, M. Selective Semihydrogenation of Alkynes with N-Graphitic-Modified Cobalt Nanoparticles Supported on Silica. *ACS Catal.* **2017**, *7* (3), 1526−1532.
(50) Van Hengstum, A. J.; Van Ommen, J. G.; Bosch, H.; Gellings, P. J. Preparation of supported vanadium and molybdenum oxide catalysts using metal acetylacetonate complexes. *Appl. Catal.* **1983**, *5* (2), 207−217.
(51) van Veen, J. A. R.; Jonkers, G.; Hesselink, W. H. Interaction of transition-metal acetylacetonates with [gamma]-Al_2O_3 surfaces. *J. Chem. Soc., Faraday Trans. 1* **1989**, *85* (2), 389−413.
(52) Toebes, M. L.; van Dillen, J. A.; de Jong, K. P. Synthesis of supported palladium catalysts. *J. Mol. Catal. A: Chem.* **2001**, *173* (1−2), 75−98.
(53) Mouat, A. R.; George, C.; Kobayashi, T.; Pruski, M.; van Duyne, R. P.; Marks, T. J.; Stair, P. C. Highly Dispersed SiO_x/Al_2O_3 Catalysts Illuminate the Reactivity of Isolated Silanol Sites. *Angew. Chem., Int. Ed.* **2015**, *54* (45), 13346−13351.
(54) Kobayashi, T.; Perras, F. A.; Slowing, I. I.; Sadow, A. D.; Pruski, M. Dynamic Nuclear Polarization Solid-State NMR in Heterogeneous Catalysis Research. *ACS Catal.* **2015**, *5* (12), 7055−7062.
(55) Lesage, A.; Lelli, M.; Gajan, D.; Caporini, M. A.; Vitzthum, V.; Miéville, P.; Alauzun, J.; Roussey, A.; Thieuleux, C.; Mehdi, A.; Bodenhausen, G.; Coperet, C.; Emsley, L. Surface Enhanced NMR Spectroscopy by Dynamic Nuclear Polarization. *J. Am. Chem. Soc.* **2010**, *132* (44), 15459−15461.
(56) Perras, F. A.; Padmos, J. D.; Johnson, R. L.; Wang, L.-L.; Schwartz, T. J.; Kobayashi, T.; Horton, J. H.; Dumesic, J. A.; Shanks, B. H.; Johnson, D. D.; Pruski, M. Characterizing Substrate−Surface Interactions on Alumina-Supported Metal Catalysts by Dynamic Nuclear Polarization-Enhanced Double-Resonance NMR Spectroscopy. *J. Am. Chem. Soc.* **2017**, *139* (7), 2702−2709.
(57) Alvarez, G. F.; Mamlouk, M.; Senthil Kumar, S. M.; Scott, K. Preparation and Characterisation of Carbon-Supported Palladium Nanoparticles for Oxygen Reduction in Low Temperature PEM Fuel Cells. *J. Appl. Electrochem.* **2011**, *41* (8), 925−937.
(58) Wang, P.; Wang, Z.; Li, J.; Bai, Y. Preparation, Characterizations, and Catalytic Characteristics of Pd Nanoparticles Encapsulated in Mesoporous Silica. *Microporous Mesoporous Mater.* **2008**, *116* (1−3), 400−405.
(59) Nefedov, V. I.; Salyn, Y. V.; Moiseev, I. I.; Sadovskii, A. P.; Berenbljum, A. S.; Knizhnik, A. G.; Mund, S. L. ESCA and X-ray spectral study of Pd(0), Pd(I) and Pd(II) compounds with triphenylphosphine ligands. *Inorg. Chim. Acta* **1979**, *35*, L343−L344.
(60) Kim, K. S.; Gossmann, A. F.; Winograd, N. X-ray photoelectron spectroscopic studies of palladium oxides and the palladium-oxygen electrode. *Anal. Chem.* **1974**, *46* (2), 197−200.
(61) Criado, J. J.; Fernandez, I.; Macias, B.; Salas, J. M.; Medarde, M. Novel chelates of Pd(II) dithiocarbamates. Spectroscopic studies and thermal behaviour. *Inorg. Chim. Acta* **1990**, *174* (1), 67−75.
(62) Wilkie, C. A.; Harworth, D. T. A ^{13}C NMR study of some metal acetylacetone complexes. *J. Inorg. Nucl. Chem.* **1978**, *40* (2), 195−197.

DOI: 10.1021/acs.chemmater.7b04909
Chem. Mater. 2018, 30, 1032−1044

(63) Kytokivi, A.; Rautiainen, A.; Root, A. Reaction of Acetylacetone Vapour with Gamma-Alumina. *J. Chem. Soc., Faraday Trans.* **1997**, *93*, 4079−4084.
(64) Note that the combination of low surface area (60 m^2/g) and low loading (0.2% w/w of acetylacetonate) render these experiments particularly challenging. In fact, this corresponds to by far the lowest coverage of surface species ever detected by solid state NMR (less than 0.002% w/w of 13C). These experiments would have been impossible using conventional NMR equipment.
(65) Légaré, P.; Fritsch, A. XPS study of transition metal/alumina model catalysts: Equilibrium and energy referencing. *Surf. Interface Anal.* **1990**, *15* (11), 698−700.
(66) Kodre, A.; Arcon, I.; Batista, J.; Pintar, A. EXAFS analysis of Pd atomic clusters. *J. Synchrotron Radiat.* **1999**, *6* (3), 458−459.
(67) Holtzclaw, H. F.; Collman, J. P. Infrared Absorption of Metal Chelate Compounds of 1,3-Diketones1. *J. Am. Chem. Soc.* **1957**, *79* (13), 3318−3322.
(68) Rasmussen, R. S.; Tunnicliff, D. D.; Brattain, R. R. Infrared and Ultraviolet Spectroscopic Studies on Ketones. *J. Am. Chem. Soc.* **1949**, *71* (3), 1068−1072.
(69) Li, T. H.; Wang, C. M.; Xie, X. G. C-H bond activation of ethylene by bare neutral palladium and platinum atoms: a theoretical investigation. *J. Phys. Org. Chem.* **2011**, *24* (4), 292−298.
(70) Cho, H.-G.; Andrews, L. Reactions of Laser-Ablated Palladium and Platinum Atoms with Ethylene: An Infrared Study of the Palladium Complex and Platinum Insertion Product Isolated in Solid Argon. *J. Phys. Chem. A* **2004**, *108* (30), 6272−6278.
(71) Liu, S.; Tan, J. M.; Gulec, A.; Schweitzer, N. M.; Delferro, M.; Marks, L. D.; Stair, P. C.; Marks, T. J. Direct Synthesis of Low-Coordinate Pd Catalysts Supported on SiO_2 via Surface Organometallic Chemistry. *ACS Catal.* **2016**, *6* (12), 8380−8388.
(72) Jezequel, M.; Dufaud, V.; Ruiz-Garcia, M. J.; Carrillo-Hermosilla, F.; Neugebauer, U.; Niccolai, G. P.; Lefebvre, F.; Bayard, F.; Corker, J.; Fiddy, S.; Evans, J.; Broyer, J.-P.; Malinge, J.; Basset, J.-M. Supported Metallocene Catalysts by Surface Organometallic Chemistry. Synthesis, Characterization, and Reactivity in Ethylene Polymerization of Oxide-Supported Mono- and Biscyclopentadienyl Zirconium Alkyl Complexes: Establishment of Structure/Reactivity Relationships. *J. Am. Chem. Soc.* **2001**, *123* (15), 3520−3540.
(73) Peterson, E. J.; DeLaRiva, A. T.; Lin, S.; Johnson, R. S.; Guo, H.; Miller, J. T.; Hun Kwak, J.; Peden, C. H. F.; Kiefer, B.; Allard, L. F.; Ribeiro, F. H.; Datye, A. K. Low-temperature carbon monoxide oxidation catalysed by regenerable atomically dispersed palladium on alumina. *Nat. Commun.* **2014**, *5*, 4885−4896.
(74) Hackett, S. F. J.; Brydson, R. M.; Gass, M. H.; Harvey, I.; Newman, A. D.; Wilson, K.; Lee, A. F. High-Activity, Single-Site Mesoporous Pd/Al_2O_3 Catalysts for Selective Aerobic Oxidation of Allylic Alcohols. *Angew. Chem., Int. Ed.* **2007**, *46* (45), 8593−8596.
(75) Otto, K.; Haack, L. P.; deVries, J. E. Identification of two types of oxidized palladium on γ-alumina by X-ray photoelectron spectroscopy. *Appl. Catal., B* **1992**, *1* (1), 1−12.
(76) Bulushev, D. A.; Zacharska, M.; Shlyakhova, E. V.; Chuvilin, A. L.; Guo, Y.; Beloshapkin, S.; Okotrub, A. V.; Bulusheva, L. G. Single Isolated Pd2+ Cations Supported on N-Doped Carbon as Active Sites for Hydrogen Production from Formic Acid Decomposition. *ACS Catal.* **2016**, *6*, 681−691.
(77) Frenkel, A. I.; Hills, C. W.; Nuzzo, R. G. A View from the Inside: Complexity in the Atomic Scale Ordering of Supported Metal Nanoparticles. *J. Phys. Chem. B* **2001**, *105* (51), 12689−12703.
(78) Agostini, G.; Pellegrini, R.; Leofanti, G.; Bertinetti, L.; Bertarione, S.; Groppo, E.; Zecchina, A.; Lamberti, C. Determination of the Particle Size, Available Surface Area, and Nature of Exposed Sites for Silica−Alumina-Supported Pd Nanoparticles: A Multitechnical Approach. *J. Phys. Chem. C* **2009**, *113* (24), 10485−10492.
(79) Keating, J.; Sankar, G.; Hyde, T. I.; Kohara, S.; Ohara, K. Elucidation of structure and nature of the PdO-Pd transformation using in situ PDF and XAS techniques. *Phys. Chem. Chem. Phys.* **2013**, *15* (22), 8555−8565.
(80) Gulmine, J. V.; Janissek, P. R.; Heise, H. M.; Akcelrud, L. Polyethylene characterization by FTIR. *Polym. Test.* **2002**, *21* (5), 557−563.
(81) Stuve, E. M.; Madix, R. J. Bonding and Dehydrogenation of Ethylene on Palladium Metal. Vibrational Spectra and Temperature-Programed Reaction Studies on Palladium(100). *J. Phys. Chem.* **1985**, *89* (1), 105−112.
(82) Özkar, S.; Finke, R. G. Palladium(0) Nanoparticle Formation, Stabilization, and Mechanistic Studies: $Pd(acac)_2$ as a Preferred Precursor, $[Bu_4N]_2HPO_4$ Stabilizer, plus the Stoichiometry, Kinetics, and Minimal, Four-Step Mechanism of the Palladium Nanoparticle Formation and Subsequent Agglomeration Reactions. *Langmuir* **2016**, *32* (15), 3699−3716.
(83) Bayram, E.; Lu, J.; Aydin, C.; Browning, N. D.; Özkar, S.; Finney, E.; Gates, B. C.; Finke, R. G. Agglomerative Sintering of an Atomically Dispersed Ir_1/Zeolite Y Catalyst: Compelling Evidence Against Ostwald Ripening but for Bimolecular and Autocatalytic Agglomeration Catalyst Sintering Steps. *ACS Catal.* **2015**, *5* (6), 3514−3527.
(84) Tempel, D. J.; Johnson, L. K.; Huff, R. L.; White, P. S.; Brookhart, M. Mechanistic Studies of Pd(II)−α-Diimine-Catalyzed Olefin Polymerizations. *J. Am. Chem. Soc.* **2000**, *122* (28), 6686−6700.
(85) Sen, A.; Lai, T. W. Oligomerization and Isomerization of Olefins by η^3-Allyl Complexes of Palladium. The Role of the Allyl Group. *Organometallics* **1983**, *2* (8), 1059−1060.
(86) Sen, A.; Lai, T. W. Catalytic Polymerization of Acetylenes and Olefins by Tetrakis(Acetonitrile)Palladium(II) Ditetrafluoroborate. *Organometallics* **1982**, *1* (2), 415−417.
(87) Delferro, M.; McInnis, J. P.; Marks, T. J. Ethylene Polymerization Characteristics of an Electron-Deficient Nickel(II) Phenoxyiminato Catalyst Modulated by Non-Innocent Intramolecular Hydrogen Bonding. *Organometallics* **2010**, *29*, 5040−5049.
(88) Sen, A.; Lai, T. W. Mechanism of Palladium(II)-Catalyzed Carbon-Carbon Double Bond Isomerization in Olefins. *Inorg. Chem.* **1984**, *23* (20), 3257−3258.
(89) Conley, M. P.; Delley, M. F.; Nunez-Zarur, F.; Comas-Vives, A.; Coperet, C. Heterolytic Activation of C-H Bonds on Cr^{III}-O Surface Sites Is a Key Step in Catalytic Polymerization of Ethylene and Dehydrogenation of Propane. *Inorg. Chem.* **2015**, *54* (11), 5065−5078.
(90) Fong, A.; Yuan, Y.; Ivry, S. L.; Scott, S. L.; Peters, B. Computational Kinetic Discrimination of Ethylene Polymerization Mechanisms for the Phillips (Cr/SiO_2) Catalyst. *ACS Catal.* **2015**, *5* (6), 3360−3374.
(91) Stephenson, C. J.; McInnis, J. P.; Chen, C.; Weberski, M. P.; Motta, A.; Delferro, M.; Marks, T. J. Ni(II) Phenoxyiminato Olefin Polymerization Catalysis: Striking Coordinative Modulation of Hyperbranched Polymer Microstructure and Stability by a Proximate Sulfonyl Group. *ACS Catal.* **2014**, *4*, 999−1003.
(92) Weberski, M. P.; Chen, C. L.; Delferro, M.; Marks, T. J. Ligand Steric and Fluoroalkyl Substituent Effects on Enchainment Cooperativity and Stability in Bimetallic Nickel(II) Polymerization Catalysts. *Chem. - Eur. J.* **2012**, *18*, 10715−10732.
(93) Berkefeld, A.; Mecking, S. Deactivation Pathways of Neutral Ni(II) Polymerization Catalysts. *J. Am. Chem. Soc.* **2009**, *131* (4), 1565−1574.
(94) Estes, D. P.; Cook, A. K.; Lam, E.; Wong, L.; Copéret, C. Understanding the Lewis Acidity of Co(II) Sites on a Silica Surface. *Inorg. Chem.* **2017**, *56* (14), 7731−7736.
(95) Estes, D. P.; Siddiqi, G.; Allouche, F.; Kovtunov, K. V.; Safonova, O. V.; Trigub, A. L.; Koptyug, I. V.; Copéret, C. C−H Activation on Co,O Sites: Isolated Surface Sites versus Molecular Analogs. *J. Am. Chem. Soc.* **2016**, *138* (45), 14987−14997.
(96) Hansen, T. W.; DeLaRiva, A. T.; Challa, S. R.; Datye, A. K. Sintering of Catalytic Nanoparticles: Particle Migration or Ostwald Ripening? *Acc. Chem. Res.* **2013**, *46* (8), 1720−1730.
(97) Wang, C.; Hu, L.; Poppelmeier, K.; Stair, P. C.; Marks, L. Nucleation and Growth Process of Atomic Layer Deposition Platinum Nanoparticles on Strontium Titanate Nanocuboids. *Nanotechnology* **2017**, *28* (18), 185704.

DOI: 10.1021/acs.chemmater.7b04909
Chem. Mater. 2018, 30, 1032−1044

(98) Wynblatt, P.; Gjostein, N. A. Supported Metal Crystallites. *Prog. Solid State Chem.* **1975**, *9*, 21−58.
(99) Parker, S. C.; Campbell, C. T. Kinetic Model for Sintering of Supported Metal Particles with Improved Size-Dependent Energetics and Applications to Au on TiO_2(110). *Phys. Rev. B: Condens. Matter Mater. Phys.* **2007**, *75* (3), 035430.
(100) Prévot, G. Ostwald ripening of three-dimensional clusters on a surface studied with an ultrafast kinetic Monte Carlo algorithm. *Phys. Rev. B: Condens. Matter Mater. Phys.* **2011**, *84* (4), 045434.
(101) Granqvist, C. G.; Buhrman, R. A. Statistical model for coalescence of islands in discontinuous films. *Appl. Phys. Lett.* **1975**, *27* (12), 693−694.
(102) Tabib Zadeh Adibi, P.; Zhdanov, V. P.; Langhammer, C.; Grönbeck, H. Transient Bimodal Particle Size Distributions during Pt Sintering on Alumina and Silica. *J. Phys. Chem. C* **2015**, *119* (2), 989−996.
(103) Harris, P. J. F. Growth and Structure of SUpported Metal Catalyst Particles. *Int. Mater. Rev.* **1995**, *40*, 97−115.
(104) Le Bars, J.; Specht, U.; Bradley, J. S.; Blackmond, D. G. A Catalytic Probe of the Surface of Colloidal Palladium Particles Using Heck Coupling Reactions. *Langmuir* **1999**, *15* (22), 7621−7625.
(105) Karimi, B.; Zamani, A.; Abedi, S.; Clark, J. H. Aerobic Oxidation Of Alcohols Using Various Types of Immobilized Palladium Catalyst: the Synergistic Role of Functionalized Ligands, Morphology of Support, and Solvent in Generating and Stabilizing Nanoparticles. *Green Chem.* **2009**, *11* (1), 109−119.
(106) Pillai, U. R.; Sahle-Demessie, E. Selective Oxidation of Alcohols by Molecular Oxygen over a Pd/Mgo Catalyst in the Absence of any Additives. *Green Chem.* **2004**, *6* (3), 161−165.
(107) Choi, K.-M.; Akita, T.; Mizugaki, T.; Ebitani, K.; Kaneda, K. Highly Selective Oxidation of Allylic Alcohols Catalysed by Monodispersed 8-Shell Pd Nanoclusters in the Presence of Molecular Oxygen. *New J. Chem.* **2003**, *27* (2), 324−328.
(108) Mori, K.; Hara, T.; Mizugaki, T.; Ebitani, K.; Kaneda, K. Hydroxyapatite-Supported Palladium Nanoclusters: A Highly Active Heterogeneous Catalyst for Selective Oxidation of Alcohols by Use of Molecular Oxygen. *J. Am. Chem. Soc.* **2004**, *126* (34), 10657−10666.
(109) Gallezot, P. Selective Oxidation with Air on Metal Catalysts. *Catal. Today* **1997**, *37* (4), 405−418.
(110) Narayanan, R.; El-Sayed, M. A. Effect of Catalysis on the Stability of Metallic Nanoparticles: Suzuki Reaction Catalyzed by PVP-Palladium Nanoparticles. *J. Am. Chem. Soc.* **2003**, *125* (27), 8340−8347.
(111) Ravel, B.; Newville, M. ATHENA, ARTEMIS, HEPHAESTUS: data analysis for X-ray absorption spectroscopy using IFEFFIT. *J. Synchrotron Radiat.* **2005**, *12* (4), 537−541.

DOI: 10.1021/acs.chemmater.7b04909
Chem. Mater. 2018, 30, 1032−1044